

# Meyer-Neldel and anti-Meyer-Neldel rule in microcrystalline silicon and silicon carbide examined with Hall measurements

Torsten Bronger, Oleksandr Astakhov, and Reinhard Carius  
*IEK-5, Research Center Jülich, Germany*

We study the electronic transport in lightly phosphorus-doped hydrogenated microcrystalline silicon ( $\mu\text{-Si:H}$ ) and nominally undoped hydrogenated silicon carbide ( $\mu\text{-SiC:H}$ ) by temperature-dependent Hall measurements. The material properties cover different crystallinities and doping concentrations. For  $\mu\text{-Si:H}$  samples, the carrier concentration is altered by electron bombardment and subsequent step-wise annealing of defects. We describe the behavior of conductivity, mobility, and carrier concentration in terms of the Meyer-Neldel rule (MNR) and anti-MNR. We present the first sample switching between them. A theoretical examination leverages the anti-MNR to describe electronic room temperature properties, and it expands the statistical shift model.

## I. INTRODUCTION

Temperature-dependent measurements of transport parameters such as carrier concentration, mobility, diffusion length etc. are an important tool for understanding transport phenomena in semiconductors. Very often these parameters exhibit thermally activated behavior. For example, the conductivity  $\sigma$  can then be calculated from its activation energy  $E_a^\sigma$  and its prefactor  $\sigma_0$  according to

$$\sigma(T) = \sigma_0 \exp(-E_a^\sigma/kT). \quad (1)$$

Here,  $T$  denotes temperature, and  $k$  the Boltzmann constant. Additionally for a set of measurements, there is often observed a phenomenon called Meyer-Neldel rule (MNR) of the form

$$\sigma_0 = \sigma_{00} \exp(E_a^\sigma/E_{\text{MN}}), \quad (2)$$

with  $\sigma_{00}$  being the Meyer-Neldel prefactor and  $E_{\text{MN}}$  being the Meyer-Neldel energy. In the Arrhenius plot, this means that the (extrapolated) temperature-dependent lines originate all at the same point  $(k/E_{\text{MN}}, \sigma_{00})$ . The case  $E_{\text{MN}} < 0$  is called anti-MNR. More generally, the MNR is visualized by plotting  $\ln \sigma_0$  versus  $E_a^\sigma$ . Eq. (2) leads to a straight line with the slope  $E_{\text{MN}}$ .

Although the MNR per se is only phenomenological, it has been used frequently for material characterization. The MNR was first described for the conductivity  $\sigma$  in oxide semiconductors.[1] Since then,  $\sigma$  has remained the primary quantity for MNR examinations, however, the list of examined materials has been extended greatly. In particular in the material complex of a-Si:H,  $\mu\text{-Si:H}$ , a-Ge:H, and  $\mu\text{-SiC:H}$ , there seems to be a universal curve  $\sigma_0(E_a^\sigma)$ , which approximates the behavior of all these materials.[2, 3] For low activation energies ( $E_a^\sigma < 200$  meV), there is anti-MNR with  $E_{\text{MN}} \approx -20$  meV,[4] and for higher activation energies, there is MNR with  $E_{\text{MN}} \approx +40$  to  $+60$  meV.[3–5] For a-Si:H, however, even strong doping can not shift the activation energies into the anti-MNR region.[3] This has been achieved, however, with TFT structures.[6]

In contrast to a-Si:H, anti-MNR has been observed for  $\mu\text{-Si:H}$ . While it was formerly assumed that only heavily-doped material may exhibit anti-MNR, it was later reported for undoped  $\mu\text{-Si:H}$  and explained with low density of grain boundaries and extended tail states.[4] But even these samples fit into the above-mentioned universal shape of  $\sigma_0(E_a^\sigma)$ .

Theoretically, the MNR in disordered silicon – in particular the dependence  $\sigma_0(E_a^\sigma)$  – is explained well with a statistical shift of the Fermi level with temperature.[7, 8] Almost all experimental examinations refer to  $\sigma$ , which is much more accessible than  $n$ . Besides, in case of a-Si:H, determining reliable temperature-dependent carrier concentrations is extremely difficult due to the sign reversal of the Hall voltage.[9] This is valid with the underlying assumption that the mobility exhibits only a weak temperature dependence. Strictly speaking, however, the statistical shift model applies to carrier concentration  $n$  rather than  $\sigma$ .

Thus, in this work we examine  $n$  in terms of MNR behavior for  $\mu\text{-Si:H}$  and  $\mu\text{-SiC:H}$  specimens, and compare with  $\sigma$ . In order to do so, we perform and analyze Hall measurements. This allows to investigate the behavior of the hall mobility  $\mu$  as well. Moreover, we compare the  $\mu\text{-SiC:H}$  results with the  $\mu\text{-Si:H}$  results.

For our experimental program, samples of different activation energies are needed. There are several ways to obtain such samples. Arguably the simplest possibility is to vary doping concentration. However, it is difficult to ensure that the samples do not vary also in other parameters in this case. Alternatively, one can use a TFT structure to vary carrier concentration[6] (accepting an inhomogeneous  $n$  perpendicular to the transport path), or one can use step-wise annealing of samples degraded by the Staebler-Wronski effect.[10]

In this study, we vary the activation energy both by variation of doping and by step-wise annealing of defects. For the latter, however, we do not use the Staebler-Wronski effect, as it is too weak in  $\mu\text{-Si:H}$ . Instead, the respective samples are degraded using electron irradiation, which has the additional benefit of a very wide range of defect density.

Beyond describing experimental results in terms of the MNR, it is important to improve our understanding of the underlying physics, which still is very incomplete. The additional data for carrier conductivity and mobility can provide new insight into this. The same is true for the inclusion of  $\mu\text{-SiC:H}$  into the investigation.

## II. MATERIALS AND METHODS

### A. Preparation of silicon samples

For this study, seven  $\mu\text{-Si:H}$  layers and one a-Si:H layer were prepared. Additionally, two  $\mu\text{-Si:H}$  layers were prepared intended for electron bombardment, see next section. All of them were deposited on roughened borosilicate glass substrates (Corning 7059) of size  $4 \times 15$  mm<sup>2</sup> using plasma-enhanced chemical vapor deposition (PECVD) at a

TABLE I. Doping and crystallinity data for the silicon samples. The “silane concentration” denotes the silane concentration in hydrogen. The first set are undegraded  $\mu\text{-Si:H}$  samples, sample A-1 is an undegraded a-Si:H sample, and the last set are  $\mu\text{-Si:H}$  samples intended for electron bombardment.

sample	doping	silane conc.	crystallinity	thickness
M-1	5 ppm	2 %	84 %	2.1 $\mu\text{m}$
M-2	10 ppm	2 %	83 %	4.0 $\mu\text{m}$
M-3	1 ppm	4 %	71 %	3.5 $\mu\text{m}$
M-4	10 ppm	4 %	74 %	3.0 $\mu\text{m}$
M-5	1 ppm	6 %	33 %	4.6 $\mu\text{m}$
M-6	10 ppm	6 %	38 %	4.2 $\mu\text{m}$
A-1	10 ppm	7 %	22 %	2.7 $\mu\text{m}$
Ma-15	15 ppm	4 %	79 %	5.0 $\mu\text{m}$
Ma-150	150 ppm	3 %	79 %	1.7 $\mu\text{m}$

TABLE II. Deposition parameters and thicknesses of the  $\mu\text{-SiC:H}$  samples.

sample	process pressure in mbar	MMS flux flux in sccm	substrate temperature in $^{\circ}\text{C}$	time in min	thickness in nm
SIC-1	0.7	6	330	200	300
SIC-2	0.5	6	460	180	230
SIC-3	0.5	10	400	75	300
SIC-4	1.1	6	400	240	280
SIC-5	10.0	6	400	180	170

plasma frequency of 95 MHz and a plasma power density of 0.07 W/cm<sup>2</sup>. The pressure in the chamber was 40 Pa, and the substrate temperature 200  $^{\circ}\text{C}$ . The deposition feed gas for the undoped films was silane diluted in hydrogen. Doping was achieved by gas admixture of PH<sub>3</sub>. The ppm values in this work refer to the gas phase concentration of the dopant gas with respect to silane.

Tab. I contains the process parameters as well as the values of crystallinity and film thickness. The crystallinity was determined by Raman scattering measurements at 647 nm excitation with the semi-quantitative estimate for the crystalline volume fraction  $I_C^{RS} = I_{520}/(I_{520} + I_{480})$ . The film thickness was estimated from the deposition rate and the film mass.

### B. Variation of defect density in the same sample

The two silicon samples Ma-15 and Ma-150 of the above mentioned were intended for degradation, i. e. generation of defects, and subsequent stepwise annealing.

Both films were exposed to a beam of 2 MeV electrons with a current density 5  $\mu\text{A}/\text{cm}^2$  in a liquid nitrogen flow cryostat at approximately 100 K.[11] Electron bombardment was performed up to a dose of  $1.1 \cdot 10^{18} \text{ cm}^{-2}$ . Afterwards, the samples were handled, transported, and stored in liquid nitrogen.

The samples were annealed in vacuum at 4 or 5 temperature steps between 50  $^{\circ}\text{C}$  and 190  $^{\circ}\text{C}$  for 30 minutes each, and measured after each annealing step. Exposure time to ambient during installation of the samples into the Hall setup was typically 3–10 minutes.

### C. Preparation of silicon carbide samples

Five samples of  $\mu\text{-SiC:H}$  were deposited using hot-wire deposition on glass substrate. The varied process parameters as well as the estimated thickness are shown in Tab. II. For all samples, the filament temperature was 2000  $^{\circ}\text{C}$  and the hydrogen flux approx. 94 sccm.[12]

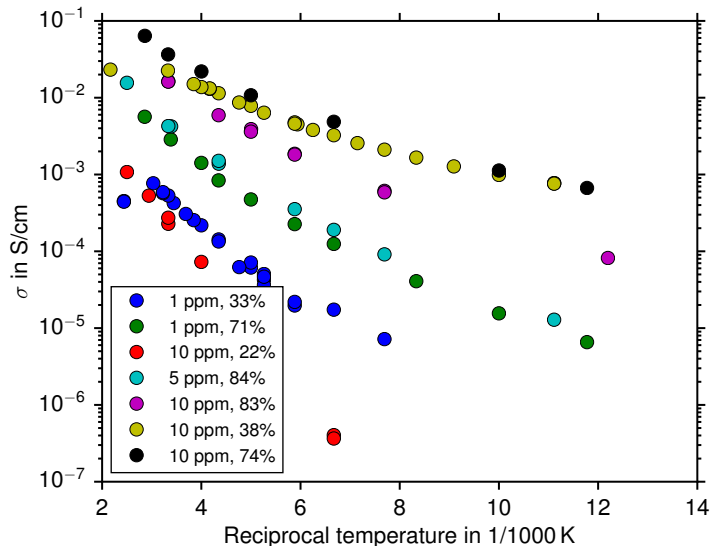


FIG. 1. Temperature-dependent conductivity for the non-degraded silicon samples.

#### D. Hall measurements

We structured and contacted the Hall samples photolithographically in order to minimize offset voltages caused by an asymmetric shape of the Hall bar. The typical Hall bar geometry was  $6 \times 1.9 \text{ mm}^2$ , having two pairs of Hall contacts.

Then, we performed temperature-dependent measurements of Hall voltage and conductivity in the range of 80–460 K. The upper limit in temperature was chosen to be well below the substrate temperature of the respective sample during deposition in order to avoid changes of the sample structure. The measurements took place in a dark, evacuated cryostat, with a magnetic flux through the sample of 1.9 T. The base voltage was 100 V.

During the measurement, the polarity of the magnetic field was switched. For both polarities, the voltages perpendicular to the electrical current were measured with electrometers with very high input resistance. Then, the difference of the average voltages at both polarities is twice the Hall voltage.[13]

### III. RESULTS

The temperature-dependent conductivity  $\sigma$ , carrier concentration  $n$ , and mobility  $\mu$  of the non-degraded silicon samples as measured with the Hall setup were already published elsewhere,[13]. For  $\sigma$ , they are reprinted in figure 1. The sign of carrier concentrations is negative in accordance with the n-type doping, except for the sample with a crystallinity of only 22%, which shows sign reversal, a well-known effect for amorphous samples.[9] Therefore, despite the non-vanishing Raman crystallinity, we will refer to this sample in the following as “amorphous”.

All three quantities increase with increasing temperature. Only above room temperature, some samples exhibit a saturation effect or even a drop in  $\mu$ , which for the non-amorphous samples is also visible in  $\sigma$  and  $n$ . The cause for it is unknown. While a similar saturation was observed in photo conductivity,[14] the explanation given therein cannot be applied here.

The curves in the Arrhenius plot are convex rather than straight, which is least pronounced in  $n$ . The root cause for this curvature is still speculative, with candidates being the statistical shift,[15] barrier height distribution,[16–19] and differential mobility.[20] In this work, we assume the first explanation, because it explains both curve shape and relative positions of the curves with the same theoretical model.

Figures 2, 3, and 4 show the Hall results for the different annealing steps of the degraded silicon sample Ma-150. The curves share the important features with those of the undegraded silicon samples, in particular the decrease to lower temperatures and the slightly convex deviation from the Arrhenius curve. The data points for  $\sigma$  are less scattered than those for  $n$  and  $\mu$ . This visualizes the previously made assertion that  $\sigma$  is the most accessible quantity. However, the noise in the Hall voltage was small enough to make the Arrhenius curves for  $n$  and  $\mu$  almost as smooth.

The figures 5, 6, and 7 depict the MNR plots of  $\sigma$ ,  $n$ , and  $\mu$  for all samples presented here (tables I and II). Every data point in an MNR plot represents an Arrhenius curve, using its slope and  $y$  intercept as coordinates. Note that

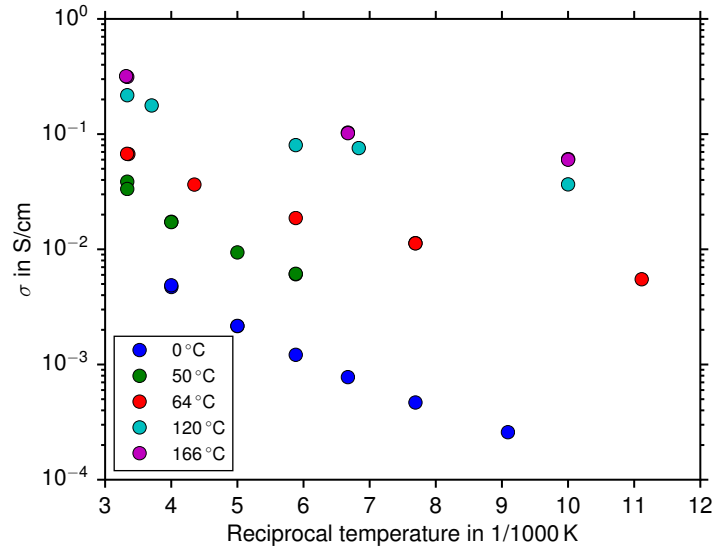


FIG. 2. Temperature-dependent conductivity for the degraded sample Ma-150, for different annealing steps.

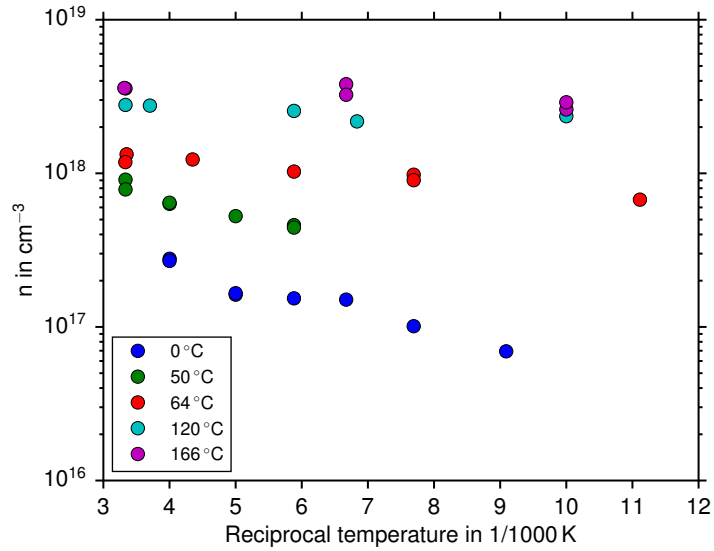


FIG. 3. Temperature-dependent carrier concentration for the degraded sample Ma-150, for different annealing steps.

because the original curves are generally not straight, an MNR plot refers to a certain temperature, in this case, room temperature. A linear slope in the MNR plot represents the existence of a Meyer-Neldel rule. The inverse of that slope is then the Meyer-Neldel energy  $E_{MN}$ . The error bars in the plots are derived from the uncertainties in slope and intersection of the straight line fit, stemming from the scattering of the data points of the Arrhenius curves.

Fig. 8 shows the dependence of the activation energies of mobility and carrier concentration. Note that this plot, too, contains all samples of this study, i. e.  $\mu\text{C-SiC:H}$ , undegraded microcrystalline silicon, undegraded amorphous silicon, and annealing steps of degraded silicon. Interestingly, most data points are positioned on the blue straight line with a slope of 1.25 and an offset of  $-18\text{ meV}$ . It is important to see that only the anti-MNR domain is covered by the ordinate. The MNR samples have much higher activation energies and do not follow this trend at all.

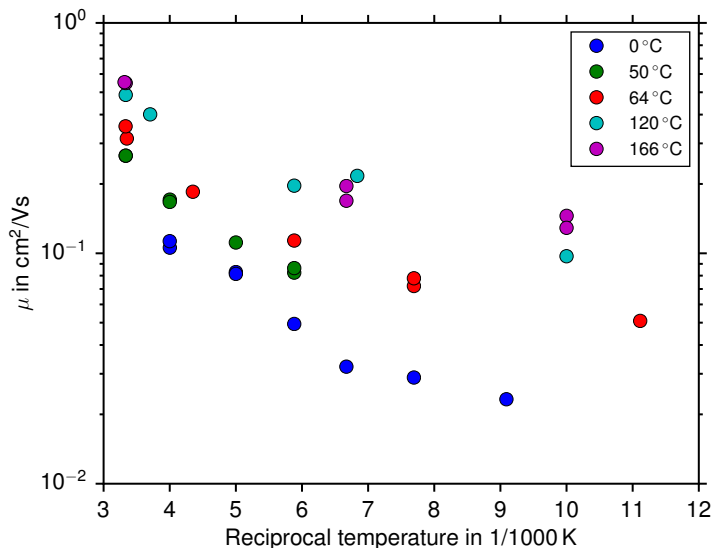


FIG. 4. Temperature-dependent mobility for the degraded sample Ma-150, for different annealing steps.

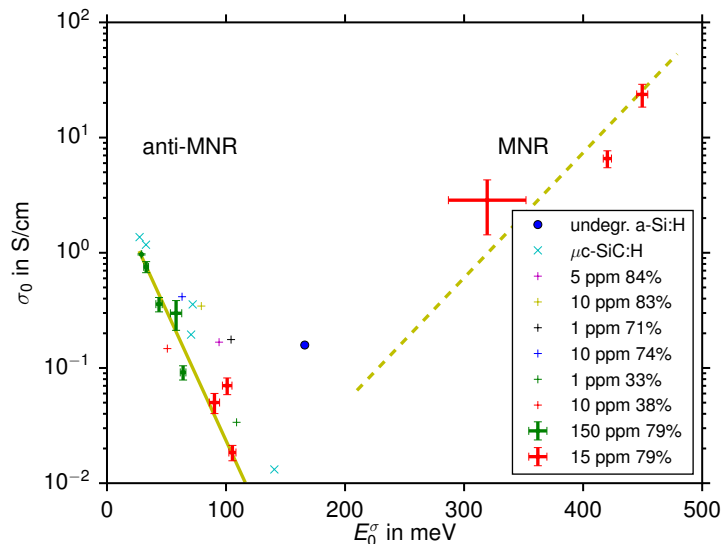


FIG. 5. MNR plot of conductivity for various measurement series. Data of the annealed samples (green and red) has error bars. The yellow solid line is a linear fit considering only the annealed samples, see Tab. III. The dashed line is only a guide to the eye, assuming an MNR trend.

## IV. DISCUSSION

### A. MNR of conductivity

As Fig. 5 shows, the behavior of the conductivity of all samples can be very well described in terms of the normal Meyer-Neldel and anti-Meyer-Neldel rules. Normal MNR, however, is only observed for some annealing steps of Ma-15. The demarcation between both lies at approx. 120 eV, which is similar to other reports.[4, 5] The amorphous silicon sample (10 ppm/22%) should also be considered being in the normal MNR regime, although it is the only representative of its type of material, so no clear classification is possible.

The majority of the samples and annealing steps presented in this work follow the anti-MNR. Two decades ago, this was restricted to highly doped crystalline material.[21] But general material quality constantly has improved since then, and so even weakly doped microcrystalline silicon can shift the Fermi level close enough to the band edge to

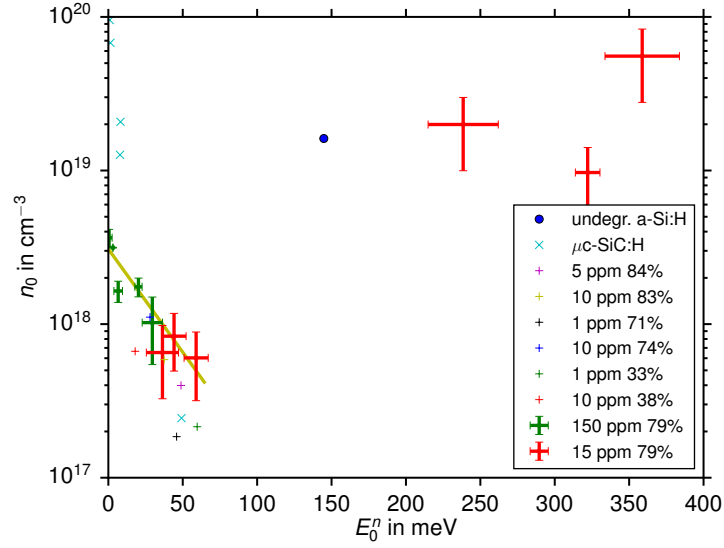


FIG. 6. MNR plot of carrier concentration for various measurement series. The yellow solid line is a linear fit considering only the annealed samples, see Tab. III. Data of the annealed samples (green and red) has error bars.

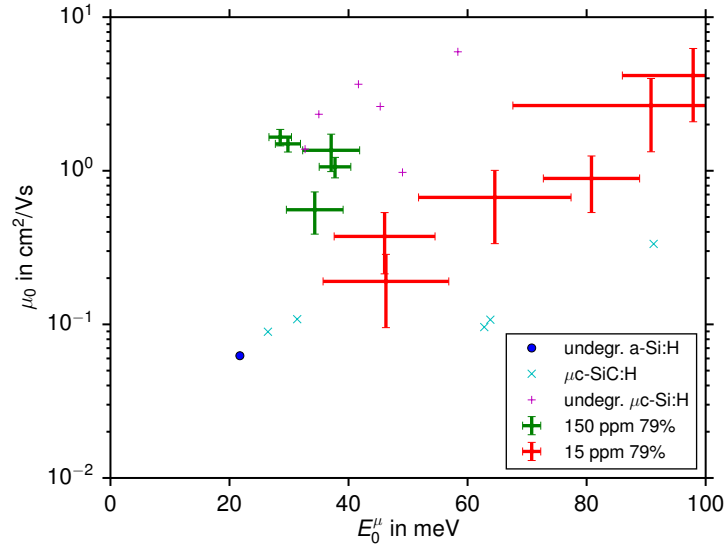


FIG. 7. MNR plot of mobility for various measurement series. Data of the annealed samples (green and red) has error bars.

reach the anti-MNR domain.[4] Obviously, the material quality of the silicon samples of this work falls in this class, too.

The  $\mu\text{C-SiC:H}$  samples fit in the general slope. To our knowledge, this is the first report of anti-MNR in  $\mu\text{C-SiC:H}$ . It is astounding that even the values of  $\sigma_{00}$  and  $E_{\text{MN}}$  correspond to those of silicon. This puts even more emphasis on the apparent – and still understood – universality of MNR plots of disordered semiconductors which has been pointed out by other authors in the past.[2, 3]

Another noteworthy result is the dichotomy of the data points of sample 15 ppm/79% in Fig. 5. The three left-hand points lie in the anti-MNR regime and follow the slope of anti-MNR. In contrast, the three right-hand points, despite the larger error estimates, clearly belong to the normal MNR regime. While such a transition was observed in a-Si:H and  $\mu\text{C-Si:H}$  by applying different gate voltages to TFT structures,[6, 22] ours is the first report of such a transition of a sample by changing material properties.

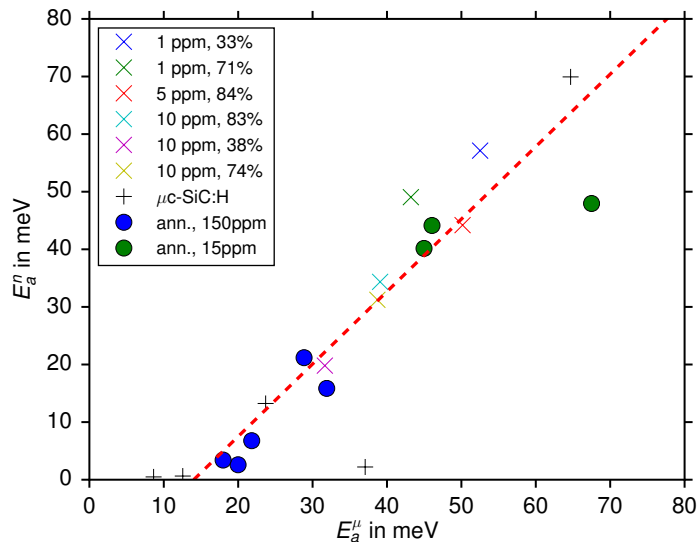


FIG. 8. Activation energy of carrier concentration versus activation energy of mobility of various measurement series. Only samples from the anti-MNR regime were taken into consideration.

### B. MNR of carrier concentration and mobility

The resulting MNR plots for  $n$  in Fig. 6 and  $\mu$  in Fig. 7 require an analysis more careful than for  $\sigma$  because uncertainties are large for many of their data points. This is due to the small Hall voltages of these samples as well as their high electrical resistance. Nevertheless, it is possible to gain information from the results.

As already explained, the model of the statistical shift of the Fermi level applies to  $n$  rather than  $\sigma$ . And indeed, Fig. 6 confirms corresponding MNR behavior of  $n$ . In the anti-MNR regime, this behavior is even more conformal for  $n$  than for  $\sigma$  comparing undegraded and degraded silicon sample series.

As the error bars indicate, the MNR data for  $\mu$  suffers from the uncertainties more than that for  $n$ . This is surprising at first since the main source of noise for both quantities is the Hall voltage, so the relative error is approximately the same. However, the activation energy interval covered by  $\sigma$  is the sum of those of  $\mu$  and  $n$ , with  $n$  taking a much greater share. Therefore, the uncertainties have much more impact on the analysis of the MNR for  $\mu$ .

Together with these uncertainties, the varying preparation conditions of the undegraded silicon samples render their data points unusable for examinations of dependences. Thus, in order to detect a trend, it is essential to keep sample variations small. This is realized by considering the annealed samples (bold red and green crosses), which reproduce the trend known from  $\sigma$  and  $n$  also for  $\mu$ . However, the uncertainties do not allow a quantitative evaluation.

### C. MNR in silicon carbide

The MNR results of silicon carbide are different from those of silicon. While the MNR of  $\sigma$  is similar to that in silicon, the anti-MNR line of  $n$  is very steep, leading to a small  $E_{\text{MN}}^n$ . At the same time,  $\mu$  exhibits no detectable MNR at all.

## V. THEORETICAL CONSIDERATIONS

### A. The significance of mobility in the MNR

The predictions of the statistical shift model[7, 8] match our observations for the carrier concentration  $n$  well. However, mostly the conductivity  $\sigma$  is experimentally examined. If the theory predicts MNR for  $n$ , but  $\sigma$  is examined for MNR behavior instead, the temperature dependence of  $\mu$  is of great significance: Since

$$\sigma = n_{00}\mu_{00} \exp\left(\frac{E_a^n}{E_{\text{MN}}^n} + \frac{E_a^\mu}{E_{\text{MN}}^\mu}\right) \exp\left(-\frac{E_a^n + E_a^\mu}{kT}\right), \quad (3)$$

TABLE III. Anti-MNR energies and  $y$  intercepts for  $\sigma$  and  $n$  for the annealed samples. For  $\mu$ , the data uncertainties were too large for evaluation.

	$E_{\text{MN}}$ (meV)	$y$ intercept
$\sigma$	-17	6.4 S/cm
$n$	-29	$3.3 \cdot 10^{18} \text{ cm}^{-3}$

one has MNR in  $\sigma$  only if

$$\frac{E_a^n}{E_{\text{MN}}^n} + \frac{E_a^\mu}{E_{\text{MN}}^\mu} = \frac{E_a^n + E_a^\mu}{E_{\text{MN}}^\sigma} + \text{terms without } E_a \text{ 's.} \quad (4)$$

This can be satisfied only if at least one of the following conditions is met:

1.  $E_a^\mu = 0$  (i. e.,  $\mu$  is temperature-independent)
2.  $E_{\text{MN}}^n = E_{\text{MN}}^\mu$
3.  $E_a^n = a \cdot E_a^\mu + b$

Here,  $a$  and  $b$  are parameters of the linear dependence. The respective MNR energies for  $\sigma$  are:

1.  $E_{\text{MN}}^\sigma = E_{\text{MN}}^n$
2.  $E_{\text{MN}}^\sigma = E_{\text{MN}}^n = E_{\text{MN}}^\mu$
3.  $E_{\text{MN}}^\sigma = (a + 1) \frac{E_{\text{MN}}^n E_{\text{MN}}^\mu}{a E_{\text{MN}}^\mu + E_{\text{MN}}^n}$

Thus, the statistical Fermi level shift is not sufficient for the occurrence of some form of MNR in  $\sigma$ . Additionally, the mobility must fulfill at least one of the three conditions.

Generally, examinations of the MNR in disordered semiconductors implicitly assume (1), i. e. a very weak temperature dependence of mobility. This stems from the theory of the mobility edge, above which electronic transport is supposed to be only sub-exponentially depending on temperature:  $\mu \sim T^{-1}$  [23]. However, this only holds if no other obstacles for the transport have significant impact. There is no direct experimental evidence for a vanishing  $E_a^\mu$  in a-Si:H, and it is certainly not true in  $\mu\text{c-Si:H}$  and  $\mu\text{c-SiC:H}$  according to figure 8.

As shown in Tab. III,  $E_{\text{MN}}^n$  exceeds  $E_{\text{MN}}^\sigma$  by a factor of 1.7. The numbers must be taken with care due to the scattering of the measurement results, but it is safe to assert that  $E_{\text{MN}}^n \neq E_{\text{MN}}^\sigma$ . Thus, condition (2) is not met at least in the anti-MNR domain.

However, the universal proportionality of  $E_a^n$  and  $E_a^\mu$  as demonstrated in Fig. 8 does fulfill condition (3). Note that for this condition, even  $E_{\text{MN}}^\mu = \infty$  is allowed, as seems to be the case for the  $\mu\text{c-SiC:H}$  samples. Unfortunately, to our knowledge, the dependence  $E_a^n \sim E_a^\mu$  hasn't been investigated or even explained hitherto. (Jackson claims in [24] that "the conductivity in a-Si:H exhibits a MNR because the statistical shift causes the carrier density to follow a MNR as well as the mobility" but the given citations do not confirm this.) The validity of this would provide great insight into transport in disordered semiconductors in general, and the MNR effects discussed here in particular.

## B. Relation between carrier concentration and mobility at room temperature

According to [13], there is a correlation between the room temperature mobility and carrier concentration  $\mu_r$  and  $n_r$  for n-doped microcrystalline silicon. The higher the doping and thus the carrier concentration, the higher the mobility. Due to the significance of these properties, there is particular interest in their inter-relation. However, no quantitative description is given.

Fig. 9 shows this dependence for the annealed samples used in this work. For 05B-054, there is a clear polynomial relation between both quantities. For 06B-276, there is no global trend. However, its three data points in the anti-MNR regime match the behaviour of 05B-054 well. Thus, despite the limited data available, it is plausible to assume a polynomial relation as well.

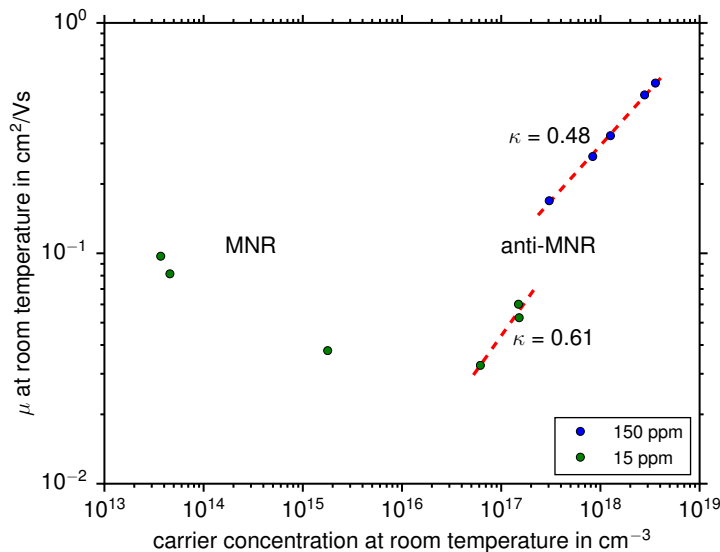


FIG. 9. The mobility versus the carrier concentration of the annealed samples, both measured at room temperature. The given values for  $\kappa$  represent the exponent of the polynomial fits (printed in dashed lines) and refer to Eq. 7.

This polynomial relation can be derived from the presence of anti-MNR and the linear dependence of the activation energies of  $n$  and  $\mu$ :

$$\mu_r(n_r) = \mu'_{00} \left( \frac{n_r}{n_{00}} \right)^\kappa \quad \text{with} \quad (5)$$

$$\mu'_{00} = \mu_{00} \exp \left( \frac{E_{\text{MN}}^\mu - kT_r}{aE_{\text{MN}}^\mu kT_r} \cdot b \right) \quad (6)$$

$$\kappa = \frac{E_{\text{MN}}^n (E_{\text{MN}}^\mu - kT_r)}{aE_{\text{MN}}^\mu (E_{\text{MN}}^n - kT_r)}, \quad (7)$$

with  $T_r$  being room temperature,  $a$  and  $b$  as defined in the previous section, and  $\kappa$  ranging between 0.5 and 1.5, in accordance with the large uncertainties in  $E_{\text{MN}}^n$  and  $E_{\text{MN}}^\mu$ . See appendix A for details of the calculation.

## VI. CONCLUSIONS

The electrical transport in disordered semiconductors was investigated by evaluating Hall measurements for a critical examination of the MNR. On the one hand, it is backed by the well-established theory of the statistical shift, and on the other hand, it allows to average many measurements, thus stabilizing the results significantly.

The splitting of  $\sigma$  into  $n$  and  $\mu$  for state-of-the-art, weakly n-doped  $\mu\text{c-Si:H}$  samples shows that all three quantities follow an anti-MNR. Moreover,  $\mu\text{c-SiC:H}$  samples exhibit anti-MNR for  $\sigma$  and  $n$  very similar to  $\mu\text{c-Si:H}$ , in both prefactor and MNR energy. The same could not be observed for  $\mu$ , but this needs to be investigated further. Furthermore, we demonstrate a switch from MNR to anti-MNR in microcrystalline silicon in the same sample by variation of its defect density, which consolidates the Fermi level position as being critical for MNR behavior.

Theoretical examination reveals that from MNR behavior in  $n$  does not necessarily follow MNR behavior in  $\sigma$ , as it is necessary for using  $\sigma$  as the observable. Instead, the temperature dependence of  $\mu$  must meet any of the conditions listed in section V A. We show that one of these conditions, namely the proportionality of the activation energies of  $n$  and  $\mu$ , is indeed fulfilled for the anti-MNR domain in both  $\mu\text{c-SiC:H}$  and  $\mu\text{c-Si:H}$ , even with the same parameters.

Finally, from this proportionality, we derive a power law relation between carrier concentration and mobility, which can be observed clearly when varying the defect density.

Further investigations should focus on the peculiar relation of mobility and carrier density. So far, the behavior of the mobility has been only described rather than understood. The proportionality of the activation energies of  $n$  and  $\mu$  appears to be crucial for the understanding of the underlying physics in the presence of anti-MNR. Other material systems should be tested for this proportionality, and whether their parameters are the same as for the material systems presented here.

### Appendix A: Derivation of $\mu(n)$ at root temperature

Let  $n_r$  and  $\mu_r$  be the respective quantity measured at  $T_r$ . Then, the activation energies are difference quotients:

$$E_a^n = \frac{\ln \frac{n_{00}}{n_r}}{\frac{1}{kT_r} - \frac{1}{E_{MN}^n}}, \quad (\text{A1})$$

$$E_a^\mu = \frac{\ln \frac{\mu_{00}}{\mu_r}}{\frac{1}{kT_r} - \frac{1}{E_{MN}^\mu}}. \quad (\text{A2})$$

Since we can connect both equations by using

$$E_a^n = a \cdot E_a^\mu + b \quad (\text{A3})$$

(see section V A), it indeed follows

$$\mu_r = \mu'_{00} \left( \frac{n_r}{n_{00}} \right)^\kappa, \quad (\text{A4})$$

with  $\mu'_{00}$  and  $\kappa$  defined as at the end of section V A.

- 
- [1] W. v. Meyer and H. Neldel, *Z. tech. Phys* **18**, 588 (1937).
  - [2] W. Fuhs, P. Kanschat, and K. Lips, *Journal of Vacuum Science & Technology B: Microelectronics and Nanometer Structures* **18**, 17921795 (2000).
  - [3] P. Thomas and H. Overhof, in *Defect and Diffusion Forum*, Vol. 192 (Trans Tech Publ, 2001) p. 114.
  - [4] S. K. Ram, S. Kumar, and P. Roca i Cabarrocas, *Journal of Non-Crystalline Solids* **354**, 22632267 (2008).
  - [5] S. K. Ram, S. Kumar, and P. R. i. Cabarrocas, in *Materials Research Society Symposium Proceedings*, Vol. 715 (Cambridge University Press, 2002) p. 357362.
  - [6] M. Kondo, Y. Chida, and A. Matsuda, *Journal of Non-Crystalline Solids* **198**, 178 (1996).
  - [7] H. Overhof and W. Beyer, *Philosophical Magazine B* **43**, 433450 (1981).
  - [8] H. Overhof and W. Beyer, *Philosophical Magazine Part B* **47**, 377 (1983).
  - [9] W. Beyer and H. Mell, in *7th Int. Conf. on Amorphous and Liquid Semiconductors*, edited by W. E. Spear (1977) p. 333.
  - [10] P. Irsigler, D. Wagner, and D. Dunstan, *Journal of Physics C: Solid State Physics* **16**, 6605 (1983).
  - [11] O. Astakhov, R. Carius, Y. Petrusenko, V. Borysenko, D. Barankov, and F. Finger, in *MRS Proceedings*, Vol. 989 (Cambridge University Press, 2007) pp. 3–8.
  - [12] F. Finger, O. Astakhov, T. Bronger, R. Carius, T. Chen, A. Dasgupta, A. Gordijn, L. Houben, Y. Huang, S. Klein, *et al.*, *Thin Solid Films* **517**, 3507 (2009).
  - [13] T. Bronger and R. Carius, *Thin Solid Films* **515**, 7486 (2007).
  - [14] S. K. Ram, S. Kumar, and P. Roca i Cabarrocas, *Journal of non-crystalline solids* **352**, 1172 (2006).
  - [15] B.-G. Yoon, C. Lee, and J. Jang, *Journal of applied physics* **60**, 673 (1986).
  - [16] J. Werner, *Solid State Phenomena* **37**, 213 (1994).
  - [17] T. Bronger, *Electronic properties of  $\mu\text{-Si:H}$  layers investigated with Hall measurements*, Ph.D. thesis, RWTH Aachen, Germany (2007).
  - [18] R. Carius, F. Finger, U. Backhausen, M. Luysberg, P. Hapke, L. Houben, M. Otte, and H. Overhof, in *MRS Proceedings*, Vol. 467 (Cambridge University Press, 1997) p. 283.
  - [19] J. C. Dyre, *Journal of Physics C: Solid State Physics* **19**, 5655 (1986).
  - [20] R. Carius, J. Müller, F. Finger, N. Harder, P. Hapke, J. Marshall, N. Kirov, A. Vavrek, and J. Maud, in *Thin Film Materials and Devices-Developments in Science and Technology* (1999) p. 157.
  - [21] G. Lucovsky, C. Wang, M. Williams, Y. Chen, and D. Mauer, in *MRS Proceedings*, Vol. 283 (Cambridge University Press, 1992) p. 443.
  - [22] H. Meiling and R. Schropp, *Applied physics letters* **74**, 10121014 (1999).
  - [23] N. F. Mott and E. A. Davis, *Electronic processes in non-crystalline materials* (Oxford University Press, 2012).
  - [24] W. Jackson, *Physical Review B* **38**, 3595 (1988).